



Article

# Research on Vehicle Frame Optimization Methods Based on the Combination of Size Optimization and Topology Optimization

Qun He <sup>1</sup>, Xinning Li <sup>2</sup>, Wenjie Mao <sup>1</sup>, Xianhai Yang <sup>1,\*</sup> and Hu Wu <sup>1</sup>

<sup>1</sup> School of Mechanical Engineering, Shandong University of Technology, Zibo 255000, China; 21501050056@stumail.sdut.edu.cn (Q.H.); 22501050048@stumail.sdut.edu.cn (W.M.); wh\_322@sdut.edu.cn (H.W.)

<sup>2</sup> School of Intelligent Manufacturing, Zibo Vocational Institute, Zibo 255000, China; 12654@zbc.edu.cn

\* Correspondence: yxh@sdut.edu.cn

**Abstract:** The efficient development of electric vehicles is essential to drive society towards sustainable development. Designing a lightweight frame is a key strategy to improve the economy and environment, increase energy efficiency, and reduce carbon emissions. Taking an automatic loading and unloading mixer truck as the research object, a force analysis of its frame was conducted under six typical working conditions. A size optimization method based on a hybrid model of the Kriging model and the analytic hierarchy process (AHP) is proposed. An approximate model of the mass and maximum stress of the frame was established using the Kriging model, and the Kriging model was optimized by using the multi-objective genetic optimization algorithm and the AHP method. Meanwhile, topology optimization was introduced to improve the structural performance of the frame and reduce its weight. The optimization results show that the overall weight of the frame is reduced by 11.96% compared to the pre-optimization period, though it still meets the material performance specifications. By comparing the iterative curves of the single Kriging model with those of the AHP model, it can be seen that the initial optimization efficiency of the hybrid model is about twice as much as that of the AHP model, and the final optimization result is improved by about 3.6% compared with the Kriging model. This validates the hybrid model as an effective tool for the multi-objective optimization of electric vehicle frames, providing more efficient and accurate optimization results for frame design.

**Keywords:** vehicle frame; size optimization; topological optimization; kriging model; analytic hierarchy process



**Citation:** He, Q.; Li, X.; Mao, W.; Yang, X.; Wu, H. Research on Vehicle Frame Optimization Methods Based on the Combination of Size Optimization and Topology Optimization. *World Electr. Veh. J.* **2024**, *15*, 107. <https://doi.org/10.3390/wevj15030107>

Academic Editors: Eric Cheng and Junfeng Liu

Received: 30 November 2023

Revised: 22 February 2024

Accepted: 6 March 2024

Published: 9 March 2024



**Copyright:** © 2024 by the authors. Licensee MDPI, Basel, Switzerland. This article is an open access article distributed under the terms and conditions of the Creative Commons Attribution (CC BY) license (<https://creativecommons.org/licenses/by/4.0/>).

## 1. Introduction

A vehicle's frame is the vehicle's skeleton and support system, and it has a significant effect on both performance and safety. The traditional method of designing frames is primarily based on expertise and trial and error, so it is less effective and cannot provide an optimal frame design. The application of finite element analysis (FEA) technology to the design of the best vehicle frames has become a research hotspot with the advancement of FEA technology. However, the current frame optimization design mainly focuses on size optimization or topology optimization and ignores the method of combining the two, which makes the frame optimization design process have certain limitations and shortcomings. Thus, this study will investigate how to combine dimensional optimization and topology optimization to optimize a mixer truck frame's design and enhance the frame's performance and safety, all based on the ANSYS Workbench 2020R2 software.

Size optimization belongs to one kind of parametric optimization technique; it is a very classical and frequently used structural optimization technique. It can reduce the system's overall weight and energy consumption and make the whole system more compact by changing the size and shape of the parts and components in the system. For instance, it can

optimize the structure's thickness, beam and rod cross sections, the moment of inertia, the stiffness of elastic elements, and other parameters. At present, the main size optimization techniques are the mathematical planning method and the optimality criterion method [1]. Sensitivity analysis is a highly effective method of performing size optimization for large and complex engineering problems.

In academic research, topology optimization is a mathematical technique. The material distribution within a designated area is optimized by taking into account specific loading conditions, constraints, and performance metrics. Finding the best material distribution path inside a predetermined design space is the main goal. This is carried out to satisfy several performance requirements and produce the lightest design possible. Homogenization, the variable thickness method, variable density method, level set method, evolutionary structural optimization (ESO), and the independent continuous mapping method (ICM) are currently widely used topology optimization techniques [2]. The variable density method, which was developed from the basis of density-based topology optimization techniques, is the most often used method. To obtain a more optimized result, the core concept is to use different density parameters in different areas of the structure.

Size optimization and topology optimization have been widely researched in recent years, with significant applications in engineering design, materials science, and other fields. Abroad, the research and application of size optimization and topology optimization are highly advanced. Currently, major foreign research institutions and scholars are employing topology optimization and size optimization methods for the design and optimization of aerospace structures, mechanical manufacturing, architectural structures, and automotive engineering. This ongoing trend continually propels the application and development of size optimization and topology optimization. Michell first proposed the concept of topology optimization in truss theory in 1904 [3], and the optimal design of structural topology, based on the homogenization theory published by Bendsoe and Kikuchi in 1988, opened a new situation in the study of optimal designs for the topology of continuum structures [4]. Soon after the homogenization theory was developed, Bendsoe introduced a density function of continuous design variables, which is also referred to as Solid Isotropic Materials with Penalties (SIMP) [5]; this allowed for the elimination of the discrete nature of the problem in many ways. The evolutionary structural optimization method was proposed by Steven GP and Xie YM in 1993 [6]. The intermediate density values in the SIMP model were properly physically interpreted by Bendsoe and Sigmund in 1999. This meant that the stiffness that could be obtained from the SIMP model could actually be realized as the stiffness of a microstructure made up of the number of solid materials corresponding to the voids and the corresponding densities. This demonstrated that density-based approaches have physical significance [7]. Many academics have been researching topology optimization in various domains in recent years. For instance, Cetin B. Dilgen et al. applied topology optimization to fluid system turbulence in 2018 and introduced the use of the automatic differentiation method for exact sensitivity in large-scale two- and three-dimensional turbulence topology optimization problems. The findings demonstrated the significance of exact sensitivity analysis and opened up new avenues for the design of turbulence-related large-scale multi-physics field problems [8]. In order to achieve design results comparable to those obtained using free-form topology optimization techniques, Julián A. Norato (2018) proposed a continuum-based structural topology optimization method, which was demonstrated to be effective by numerical examples [9]. In 2019, I. Sosnovik and I. Oseledets proposed a neural network as an efficient tool for accelerating the topology optimization process that significantly reduces the optimization time consumption [10]. Pedro Gomes and Rafael Palacios (2020) investigated the use of topology optimization in the elastic and aerodynamic design of flexible wings. They used a geometrically nonlinear finite element structural solver in conjunction with a Reynolds-averaged Navier–Stokes finite volume solver [11].

The history of size optimization development can be traced back to the 1960s. With the development of computer technology and finite element analysis methods, size optimization methods have been gradually introduced into the engineering field and have

been widely applied and studied. In the late 1960s and early 1970s, the earliest size optimization methods mainly used some direct optimization methods, such as the variable load, stiffness matrix, direct deformation method, and so on. The main advantage of these methods is that they are easy to understand and implement, but they are limited by computational power and accuracy. By the mid-1970s, with the development of digital computers and the application of the finite element method, size optimization methods began to enter a new stage of theory and practical application. Currently, the majority of size optimization techniques are based on finite element methods and are optimized through mathematical planning techniques, like strength assumptions, as demonstrated by Koiter [12]; optimization methods for elastic structures, as demonstrated by Pian and Sumihara [13]; as well as feasible domain methods, as demonstrated by Rozvany [14]. After the 1980s, size optimization methods were further developed, and methods based on variable transformation and sensitivity analysis appeared; these techniques include the Lagrangian method, the proposed Newton method, the coefficient optimization method, and others. The main advantages of these methods are their high efficiency and flexibility, which can effectively solve some practical engineering problems. Also, there are some important works in this phase, such as the finite element substructure and spatial lattice grid methods proposed by Arora and Cheng [15], and the multi-objective optimization methods proposed by Svanberg and Sobieszczanski-Sobieski et al. [16]. From the 1990s to the present, size optimization methods have been widely used, especially in industry. With the rapid development of computer technology, the speed of size optimization calculation has been significantly improved. In addition, cross-research with the fields of mechanics of materials, engineering mechanics, and computer science has also received extensive attention. At this stage, the research focus shifted to multi-objective optimization, structural optimization, optimal design, and multidisciplinary optimization. Meanwhile, with the development of advanced computer technology and optimization algorithms, the application prospect of size optimization will become broader and provide strong support for practical engineering applications.

In addition, in recent years, electric vehicles, as part of renewable energy, have become important components of energy sustainability. The rise of electric vehicles brings new challenges and opportunities for energy management. In a multi-energy hybrid system, more intelligent, flexible, and sustainable energy utilization can be achieved by effectively integrating resources such as combined heat and power (CHP), green energy, fuel cells, and plug-in electric vehicles (PEVs). Some advanced adaptive control strategies, such as the proposed Optimal Self-Tuning Fractional Order Fuzzy Controller (OSTFOF), offer new possibilities for the performance of electric vehicles in terms of resource savings. This controller optimally tunes its parameters by means of a path-finding algorithm (PFA) to adaptively obtain proportional, integral, and derivative gain values to account for nonlinearities, such as governor dead zones and power generation rate constraints, in a combined heat and power system. The simulation results show that the proposed OSTFOF controller exhibits excellent performance metrics in various scenarios compared to the conventional PI, PID, and FOPID controllers, and it provides strong support for the sustainable development of electric vehicles in the energy system [17]. In addition, with the wide application of electric vehicles, the bidirectional power control of EV aggregators is not only regarded as an innovation, but also as an intelligent choice for distributed energy storage. This control strategy not only flexibly adjusts the energy flow in the grid, but also effectively reduces frequency and power fluctuations, providing a reliable and effective solution for the stable operation of power systems [18]. Another way to save energy is to rationally schedule the energy consumption of electric vehicles. In order to explore the impact of electric vehicle charging/discharging decisions on energy scheduling, the problem is modeled as a two-stage optimization problem. In the first stage, the main demand of EV owners is introduced as the objective function; in the second stage, the total energy cost and emission factor are considered as the main criteria. The decision variables include the generation schedules of distributed generation (DG) technologies and

the charging/discharging schedules of EVs, for which some effective modeling methods are introduced for the uncertainty of these variables. The results of the study show that it is possible to strike an effective balance between emission factors and system energy costs, emphasizing the importance of this integrated energy dispatch framework [19]. From an integrated perspective, electric vehicles play active roles in energy management and resource utilization, contributing not only to the achievement of energy sustainability but also to the construction of a more environmentally friendly and sustainable energy future. This all-encompassing impact demonstrates the enormous potential of electric vehicles to contribute to sustainable development.

Compared with foreign countries, domestic research on size optimization and topology optimization has had a late start. However, with the rapid development of China's manufacturing industry in recent years, the application of size optimization and topology optimization in engineering design and manufacturing has gradually increased, and related research and application in China has also gradually emerged. Currently, some domestic research institutions and universities have begun to carry out research on size optimization and topology optimization, involving aerospace, automotive engineering, building structures, and other fields. At the same time, some enterprises have begun to use these methods for product design and manufacturing, which promotes the development of size optimization and topology optimization technology. The development of domestic topology optimization can be traced back to the late 1980s and early 1990s, when it was mainly engaged in the research of structural topology design. In the late 1980s and early 1990s, this stage was mainly led by scholars at home and abroad, and the theoretical foundation of structural topology optimization was gradually established, but it was mainly based on the research of a two-dimensional model, which was relatively simple and rough. By the early 2000s, a period of rapid development of topology optimization research began in China. Drawing from the results of advanced research conducted abroad, domestic scholars started conducting a great deal of research using techniques like the MMA method, SIMP method, LP planning, etc. [20]. At this point, domestic researchers also started looking into the use of topology optimization in engineering applications, including ship structures, mechanical parts, automotive parts, and other areas. Between 2000 and 2010, researchers in the country started using topology optimization for more intricate structural designs, consisting of microscale, nonlinear, and multi-physics field optimization. Furthermore, a few topology optimization programs, including TOGO and TOMO, started to surface in China [21]. In China, topology optimization finally reached the stage of multidisciplinary integration since 2010 [22]. This includes applications in the fields of construction, subterranean engineering, electronic circuits, and machinery in addition to aerospace, aviation, and other fields. Additionally, some new topology optimization methods, like Hybrid Element Topology Optimization (HETOP) [23], have emerged in recent years, which are expected to provide better solutions for more complex structural designs.

It is evident from the aforementioned analysis that most current research on vehicle frame optimization is conducted in one of two directions: size optimization or topology optimization. However, very few studies take into account both of these factors in their entirety. Topology optimization focuses on the rationality of shape and the efficient use of materials, yet it frequently encounters the issue of insufficient structural stiffness in real-world engineering applications. Size optimization seeks structural compactness and stiffness; nevertheless, pursuing only stiffness may result in an unneeded increase in weight. Performance trade-offs can easily result from the two being optimized separately. To create a lightweight vehicle frame that still maintains adequate stiffness and strength, this study tries to investigate the natural fusion of size optimization and topology optimization. The ultimate goal is to offer a more creative and effective solution for the long-term advancement of automotive engineering. This paper's primary research involves the following:

- (1) An automatic loading and unloading mixer truck is used as an example to thoroughly examine a mixer truck's overall load-bearing performance; to carry out a multi-case

stress analysis and static finite element analysis; to identify the riskiest operating circumstances; and to study structural modal characteristics before vehicle frame optimization.

(2) A sensitivity analysis is used to filter out the important structural parameters and design variables that significantly affect a vehicle's frame weight; structural static characteristics as well as structural modal characteristics are chosen. The Kriging method is used to create an approximate model of the vehicle's frame weight and maximum stress. After that, the multi-objective genetic algorithm is combined with the hierarchical analysis method to optimize the vehicle frame with the goals of minimum mass and maximum stress.

(3) The size and topology optimization techniques are combined to fully optimize the vehicle frame's structural parameters. Ultimately, the optimized frame's simulation and experiments confirm its dependability under a range of operating conditions and show off the frame's outstanding performance under a load.

## 2. Optimization Strategy

### 2.1. Optimization Process

Firstly, this paper takes an automatic loading and unloading mixer truck frame as an example; the primary loads of the mixer truck frame are obtained; and a 3D simulation model is built in Solidworks 2021 software using the real model as a basis. The model is then loaded into ANSYS Workbench for processing and simplification. Four representative working conditions are chosen for this paper's in-depth analysis of the mixer truck's operating conditions: (a) bucket raised static state; (b) bucket flat static state; (c) uphill 15 degrees; and (d) downhill 15 degrees. The force of the fully loaded mixing tank on the frame of the aforementioned four working conditions is calculated based on the actual load situation on the frame. The vehicle frame's finite element model is then created in the ANSYS Workbench 2020R2 software, and its force and deformation under various working conditions are analyzed using finite elements to identify the working condition with the greatest force and deformation. This information serves as the foundation for the topology and size optimizations that follow. This paper first performs a rigorous verification of the size optimization of a few vehicle frame segments. To determine the final vehicle frame optimization scheme, the optimized vehicle frame is again put through topology optimization after passing the verification. Figure 1 depicts the comprehensive optimization technology route.

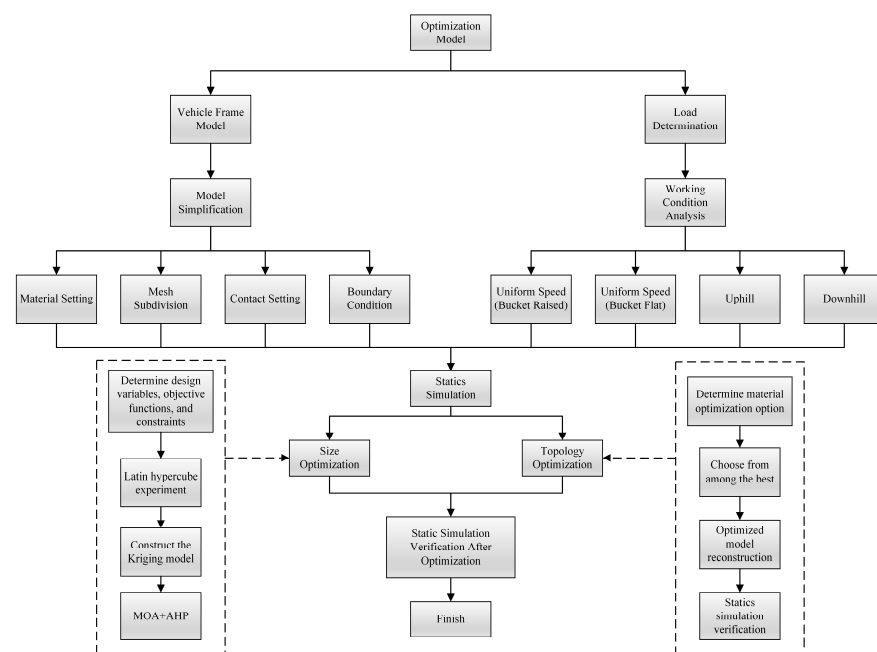


Figure 1. Technical route.

## 2.2. Multi-Objective Vehicle Frame Size Optimization

As the complexity of engineering problems increases, the simulation model becomes more complex and larger in scale, the time-consuming solution increases exponentially, and it will consume a large number of resources to apply the multi-objective optimization algorithms directly to the actual simulation model with physical significance, so there is an urgent need to introduce efficient multi-objective optimization methods. The computational results of the surrogate model are very close to the actual simulation model, and the solution is less computationally intensive. The surrogate model is built using a data-driven bottom-up approach. The following three steps are used to construct the surrogate model [24]:

- (1) A suitable experimental design methodology is chosen to gather preliminary sample points to build the surrogate model;
- (2) An appropriate surrogate model or models are selected for use in approximating the representation data;
- (3) The constructed surrogate model or models are applied.

The Kriging model, Artificial Neural Networks (ANNs), Radial Basis Functions (RBFs), Support Vector Machines (SVMs), Polynomial Regression models (PRG), and other surrogate models are more frequently used. The Kriging model has the following two characteristics [25]: (1) high prediction accuracy and (2) the ability to provide estimates of prediction accuracy. The Kriging model is becoming more and more valued in practical applications, so the Kriging model is used for size optimization in this paper.

The Kriging model consists of two models, a parametric model, which is essentially a regression analysis model, and a nonparametric model, which is essentially a stochastic distribution with the following formula:

$$y(x) = f(x)\beta + z(x) \quad (1)$$

where  $z(x)$  is a Gaussian stochastic function, and the more  $z(x)$  trends to 0, the smoother the fitting curve is;  $y(x)$  is the function estimate of the unknown point;  $\beta$  is the regression coefficient; and  $f(x)$  is a linear regression function that conforms to the expectation of the global function, which is used to model the expectation function of the stochastic process, usually using polynomials. The following characteristics of  $z(x)$  are as follows:

$$E[z(x)] = 0 \quad (2)$$

$$Var[z(x)] = \sigma^2 \quad (3)$$

$$Cov[z(x_i), z(x_j)] = \sigma^2 R[R(x_i, x_j)] \quad (4)$$

Assume that  $f(x)$  is the established estimator  $\hat{f}(x)$ :

$$\hat{f}(x) = w(x)^T Y \quad (5)$$

where  $w = (w_1, w_2, \dots, w_n)^T$  is the vector of weighting coefficients to be solved;  $y = (y^1, y^2, \dots, y^n)^T$  represents the known sample point data.

For  $\hat{f}(x)$  to achieve an unbiased estimation of  $f(x)$ , it needs to be satisfied as follows:

$$E[\hat{f}(x) - f(x)] = E[w^T Y - f] = w^T G - g = 0 \quad (6)$$

where  $G = (g(x^1), g(x^2), \dots, g(x^n)^T)$ , and the above equation can be converted to

$$G^T w(x) = g(x) \quad (7)$$

Next, the variance that results from estimating  $f(x)$  using  $\hat{f}(x)$  is as follows:

$$\varphi(x) = E \left[ \left( \hat{f}(x) - f(x) \right)^2 \right] = E \left[ \left( w^T Z - z \right)^2 \right] = \sigma^2 \left( 1 + w^T R w - 2w^T r \right) \quad (8)$$

where  $R = [R_{ij}] = [R(c, x^i, x^j)]$ ,  $(i, j = 1, 2, \dots, n)$ ;  $r = (R(c, x, x^1), \dots, (R(c, x, x^n)))^T$ ; and  $R(c, x, x^i)$  is the correlation function determined using the kernel function as the Gaussian function.

$$r(d_j) = \exp \left( 1 - \frac{d_j^2}{c_j^2} \right) \quad (9)$$

where  $d_j$  denotes the distance between the point to be measured and the sample point;  $c_j$  is the constant covariate of the kernel function in the  $j$ th direction of the sample point.

Since the Kriging response surface model requires the estimation variance to be minimized, i.e., the weighting coefficients  $w$  are minimized, the final solution yields the final results as follows:

$$w(x) = R^{-1} \left[ r(x) - G \left( G^T R^{-1} G \right)^{-1} \left( G^T R^{-1} r(x) - g(x) \right) \right] \quad (10)$$

$$\hat{f}(x) = g(x)\beta^* + r(x)^T \gamma^* \quad (11)$$

where  $\beta^* = (G^T R^{-1} G)^{-1} G^T R^{-1} Y$ ,  $\gamma^* = R^{-1} (Y - G\beta^*)$ .

In size optimization, commonly used constraints include mandatory constraints and feasible constraints. The mandatory constraints are the conditions that must be satisfied by the design, such as the minimum size, the maximum size, and the maximum allowable stress of the structure. The feasible constraints are the conditions that need to be satisfied by the design but are allowed to be violated to a certain extent, for example, the range limitations of the design variables, the range requirements of the natural frequency, etc. The following represents the fundamental size optimization mathematical model:

$$\begin{cases} \min f(x) \\ \text{s.t. } c_i(x) \leq 0, i = 1, 2, \dots, m \\ h_j(x) = 0, j = 1, 2, \dots, p \\ x_{\min} \leq x \leq x_{\max} \end{cases} \quad (12)$$

where  $f(x)$  is the optimization objective function,  $x$  is the vector of design variables,  $c_i(x)$  and  $h_j(x)$  are the inequality constraint and equation constraint functions, respectively, and  $x_{\min}$  and  $x_{\max}$  are the lower and upper bounds of the design variables, respectively.

### 2.3. Multi-Objective Vehicle Frame Topology Optimization

Rearranging the material's arrangement in a structure is a technique known as topology optimization. In topology optimization, a structure is usually viewed as a collection of many small units called elements. These elements can be discrete or continuous, and they can take on various shapes in various dimensions, including points, lines, surfaces, and bodies. Finding the best possible structural arrangement to minimize the structure's qualitative metrics—such as volume, mass, stiffness, frequency, and so forth—is the aim of topology optimization. Therefore, the problem of topology optimization can be viewed as a topology design problem with the goal of determining the ideal topology. The following mathematical formula can be used to express the topology optimization goal:

$$\left\{ \begin{array}{l} \rho = (\rho_1, \rho_2, \rho_3 \dots, \rho_n) \in C \\ \min m = \sum_{i=1}^n \rho_i V_i \\ \text{s.t. } S \leq 235 \text{ Mpa} \\ G \leq 0.001175 \\ 0 \leq \rho_{\min} \leq \rho_i \leq 1 \quad i = 1, 2, \dots, n \end{array} \right. \quad (13)$$

where  $\rho$  is the design variable;  $\rho_{\min}$  is the minimum density;  $\rho_i$  is the relative density;  $V_i$  is the relative volume;  $m$  is the objective function, i.e., the overall mass of the mixer truck frame;  $S$  and  $G$  are the stresses and strain to which the frame is subjected, respectively; and  $C$  is the topology-optimized design domain of the frame.

### 3. Automatic Loading and Unloading Mixer Truck Structure and Force Analysis

#### 3.1. Main Structure of Automatic Loading and Unloading Mixer Trucks

Automatic loading and unloading mixer trucks have four wheels and are capable of handling a wide range of challenging road conditions. They are also well suited for construction projects in rural areas, as their sturdy intersection-style bodies can solve water-related issues without requiring the worker to search for a power source. The main components of the entire truck are the water tank, bucket, chassis, upper and lower frames, cab, and mixing tank. The actual diagram of a concrete mixer truck is shown in Figure 2.

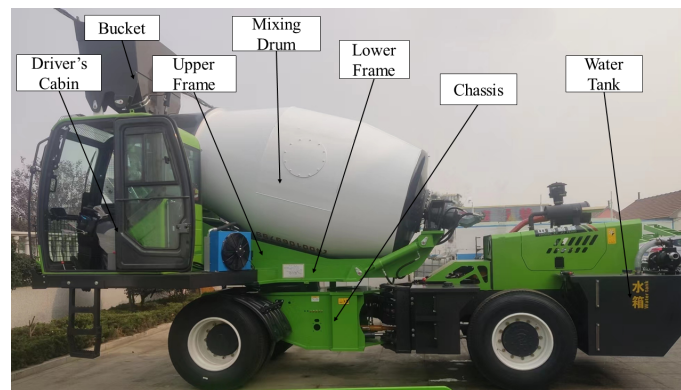


**Figure 2.** Automatic loading and unloading mixer truck with size of 3 m<sup>3</sup>.

#### 3.2. Distribution of Main Loads

The main part of the mixer truck frame is mainly composed of the upper frame (bearing the mixing cylinder) and the lower frame. The hydraulic cylinder and its pin serve as the connecting elements between the two frames. The frame primarily supports the weight of the bucket, the driver's cabin, the mixing cylinder, and the concrete. The total loads of the truck are displayed in Table 1 below.

**Table 1.** Main loads of mixer truck.

Serial Number	Load Name	Load Size/N
1	Concrete	70,560
2	Empty mixing drum (including its accessories, etc.)	8820
3	Driver's cabin	7840
4	Bucket and its contents	9800
5	Water tank	7056

#### 3.3. Analysis of Forces on Mixer Truck

As seen in the mixer truck force sketch in Figure 3, the moment equilibrium method is used to calculate the force of the mixing tank pallet of the frame to simplify the analysis of

the four typical working conditions of uphill and downhill in fully loaded work, bucket lifting, and leveling in the stationary state. It is obtained from  $\Sigma F_x = 0$ ,  $\Sigma F_y = 0$ ,  $\Sigma F_z = 0$ :

$$F_{Ax} + MA_x + MA_y \sin \theta - N_B \sin \alpha = 0 \quad (14)$$

$$F_{Ay} + MA_y \cos \theta + N_B \cos \alpha = 0 \quad (15)$$

$$F_{Az} + MA_z + F_{Bz} = 0 \quad (16)$$

Taking the moment  $\Sigma M_{Ay} = 0$  for the Y-axis force at frame A yields

$$-MA_y \cos \theta l_1 + N_B \cos \alpha (l_1 + l_2) = 0 \quad (17)$$

Taking the moment  $\Sigma M_{Az} = 0$  for the Z-axis force at frame A yields

$$MA_z l_1 + F_{Bz} (l_1 + l_2) = 0 \quad (18)$$

In the above equation,  $F_{By} = N_B \cos \alpha$ ,  $F_{Bx} = N_B \sin \alpha$ ,  $M$  is the mass of the mixing cylinder when it is fully loaded,  $l_1 = 1308$  mm,  $l_2 = 1425$  mm,  $A_x$  is the gravitational acceleration parallel to the X-axis,  $A_y$  is the gravitational acceleration parallel to the Y-axis, and  $A_z$  is the parallel Z-axis of the gravitational acceleration;  $\theta = 0^\circ$  when moving at a uniform speed on level ground,  $\theta = -15^\circ$  when moving uphill, and  $\theta = 15^\circ$  when moving downhill. When the bucket is lifting up the material, the foremost end of the bucket coincides with the frame, and the distance between the foremost end of the bucket and the frame connection can be obtained as  $l_3 = 0$  mm; the whole torque reaches the maximum when the bucket is placing the shoveling material flatly, and the distance between the bucket and the frame connection can be obtained as  $l_3 = 2300$  mm, and then two torques to the frame connections on both sides can be calculated, namely, the torque  $M_C = 22.54 \times 10^6$  N·mm and the two vertical downward forces  $F_{cy} = 4900$  N, and the rest of the forces on the frame are the same as those in Equations (14)–(18).

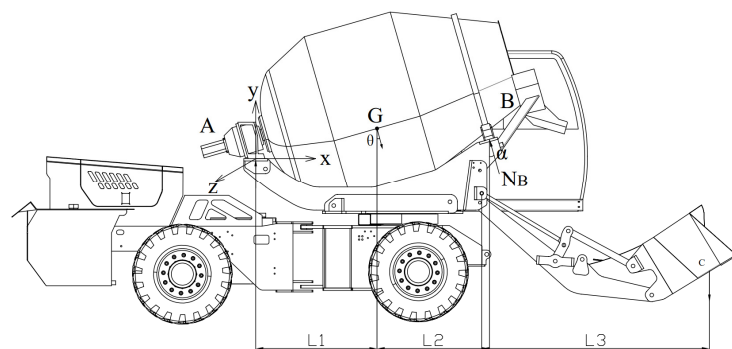


**Figure 3.** A sketch of the forces on the mixer truck. (A-Reducer support plate, B-Pallet bracket plate, C-Bucket, G-Gravity, NB-The angle of intersection of the normal to the contact point of the pallet and the mixing drum with the YZ plane,  $\theta$ -the angle up and down the slope).

## 4. A Performance Analysis of the Vehicle Frame before Optimization

### 4.1. Finite Element Modeling

#### 4.1.1. Simplified Model and Material Setup

While creating the three-dimensional digital model of the vehicle frame, it is possible to reasonably simplify the structure of the frame, because it has more intricate features, in accordance with the real circumstances. After modeling the frame individually according to the mixer truck in kind, a three-dimensional model, shown in Figure 4, is created with a total length of 2700 mm, a width of 1000 mm, and a mass of 1292.8 Kg, mainly composed of the upper frame and lower frame (including the cab). The upper frame mainly consists of two left and right tank arms and mixing tank pallets, and the lower frame mainly consists of cab pallets and turntable pallets. Q235b and 45 steel make up the majority of the frame's

materials, including the tank arm, reducer pallet, and other components. The material of 45 steel is used for the hydraulic cylinders and pins; Table 2 below lists the material property values for this material.

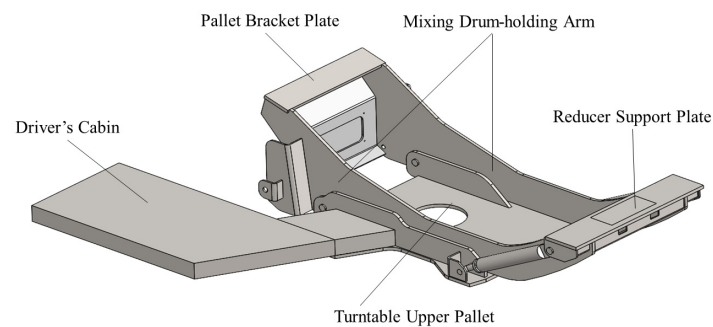


**Figure 4.** Three-dimensional model of frame.

**Table 2.** Material setting.

Material	Elastic Modulus	Yield Stress	Density	Poisson's Ratio
Q235b	200 GPa	235 MPa	7850 kg·m <sup>-3</sup>	0.3
45 Steel	209 GPa	350 MPa	7890 kg·m <sup>-3</sup>	0.269

#### 4.1.2. Mesh Generation and Mesh Validation

In this paper, a tetrahedral mesh was used to mesh the frame, generating 294,094 nodes and 150,012 finite elements. First, a default division was applied to the frame, generating approximately 60,000 finite elements. Mesh independence validation was performed to avoid a large impact of mesh sparsity on the computational results and to avoid an excessive consumption of computational time. Seven sets of meshes with different sparsity levels of nearly 60,000, 80,000, 90,000, 120,000, 140,000, 155,000, and 160,000 were created for validation in the mesh division, as shown in Figure 5a. The maximum stress of the frame is presented with the number of meshes, and after the sixth set, the deviation of the mesh calculation is less than 5%, which has less influence on the calculation results. Therefore, the sixth set of meshes, i.e., around 155,000 finite elements, was considered relatively appropriate.

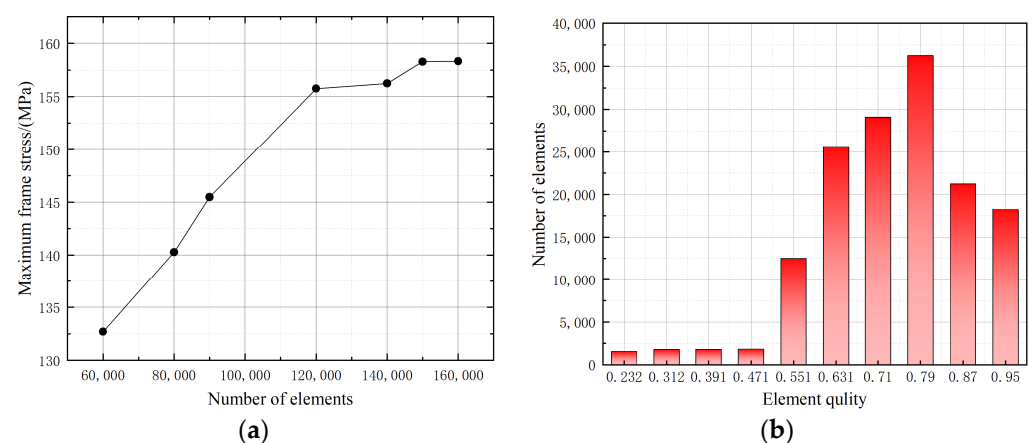


**Figure 5.** Mesh generation and mesh validation. (a) Mesh independence validation. (b) Mesh quality validation.

Next, the mesh quality was checked, as shown in Figure 5b. The results show that the number of mesh quality greater than 0.5 accounts for 95% of the total number of meshes, and most of them are concentrated around 0.8. There are very few mesh qualities lower than 0.5. This shows that the mesh quality is qualified.

#### 4.1.3. Setting of Contact Conditions, Loads, and Restraints

After importing the frame into ANSYS for meshing, the contact setup for each component of the frame is started. Firstly, the components connected at the hinge points are connected by friction, e.g., the connection between the upper frame and the lower frame. In addition, the connection of the hydraulic cylinder also involves friction connection. The other remaining parts are bound connections. The next step is to set the constraints of the frame; since only the upper part of the mixer truck is analyzed, the part of its lower frame in contact with the pallet shaft is set as Fixed support, and finally, the loads of the frame are set, as shown in Table 1. The frame is mainly subjected to the forces of concrete, mixing cylinder, cab, and bucket, so the final settings of the contact conditions, loads, and constraints of the frame are shown in Figure 6.

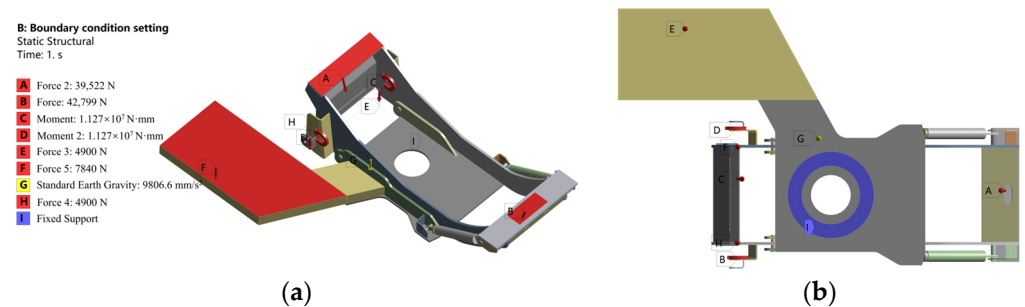


**Figure 6.** Settings of contact conditions, loads, and restraints. (a) Load application. (b) Fixed support.

#### 4.2. Strength Analysis of Frame under Different Working Conditions

Four typical working conditions were chosen for the static strength analysis. According to GB/T 26408-2011 [26], the concrete mixer truck must undergo a climbing test, in which the mixing drum must be filled to the designated capacity with concrete, the mixer truck's discharge port must face the direction of the downhill slope through a slope of at least 14%, and the concrete must not overflow. Therefore, the selected working conditions are a mixer truck at rest with the bucket raised; a mixer truck at rest with the bucket flat; and 15 degrees uphill and 15 degrees downhill. After importing the aforementioned finite element model into ANSYS, the maximum stress cloud of the frame is obtained, and it is displayed in Figure 7. The maximum stress is found when the bucket is placed flat at the stationary state in working condition b, according to the stress cloud analysis of these four working conditions. The front end of the mixing tank pallet bears the majority of the larger stresses in the arm portion of the frame. Thus, the maximum stress value when the bucket is placed flat in condition b is considered to construct the Kriging model.

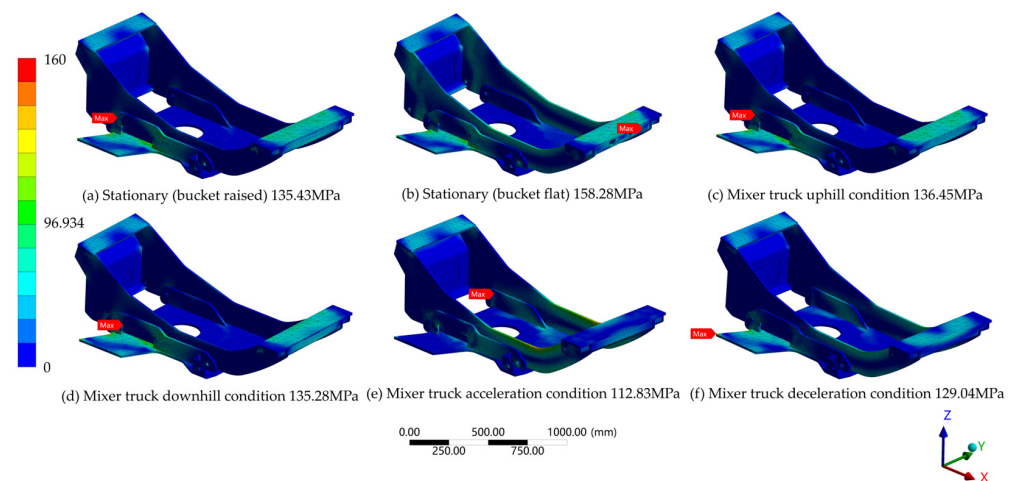


**Figure 7.** Maximum stress diagrams for each working condition of the frame.

### 4.3. Frame Modal Analysis

When the mixer truck is working, its frame will be subjected to a variety of external excitation frequencies; if the external excitation frequency is close to the frequency of the frame itself, it will trigger the resonance phenomenon, resulting in the deformation of the frame, and even causing damage to occur. For this reason, it is important to confirm the frame's dynamic characteristics as well as whether they remain reasonable following further optimization. The following are common guidelines for assessing the frame when using the modal analysis method [27]:

- (1) The value of the intrinsic frequency of the low-order modes of the vehicle frame should be lower than the operating frequency of the engine when idle to avoid the overall resonance phenomenon;
- (2) The elastic mode frequency of the vehicle frame should try to avoid the frequency so that the engine often works;
- (3) The vibration pattern of the vehicle frame should be as smooth as possible to avoid sudden changes.

The mixer truck uses a four-cylinder engine with a rated power of 85 Kw, and its frequency is about 25 Hz at when the engine is idle and 70 Hz at a common speed. Through the first 15 orders of the frame modal analysis, as shown in Table 3, 1–6 orders are rigid body modes, the frequency of the first 10 orders are lower than the frequency of the engine when it is idle, and the frequency of the last 5 orders are also lower than the frequency of the engine when in common use. From Table 3, it can be seen that the frame of each order of the frequency change is stable, and there is no prominent phenomenon. Based on the above analysis, the design of the frame is reasonable and meets the requirements of the vehicle.

**Table 3.** Fifteenth-order modal analysis of frame.

Ordinal Number	Frequency/Hz
1~6	0
7	8.94
8	16.7
9	19.5
10	23.2
11	25.2
12	27.8
13	30.3
14	32.5
15	39.8

## 5. Mixer Vehicle Frame Size Optimization

### 5.1. Selection of Design Variables

The choice of suitable design variables is an important stage in the lightweight frame design process, and it has a direct impact on the effectiveness and performance of the finished design. Eight design variables were chosen in total: P1 and P2 denote the frame's left and right tank arms; P3 and P4 denote the exterior frame's left and right reinforcing plates; P5 and P6 denote the wheel carrier pallets and reducer pallets, respectively; and P7 and P8 denote the interior frame's left and right reinforcing plates. The sensitivity analysis, as illustrated in Figure 8, revealed that the primary four design variables—P1, P2, P3, and P4—have a greater impact on the major performance metrics, including the weight, the frame's deformation, maximum stress, and strain. As a result, when optimizing the lightweight design of the frame, the main attention and resources should be focused on these design variables to ensure that the final design solution can reduce the weight while maintaining the structural strength and performance of the frame.

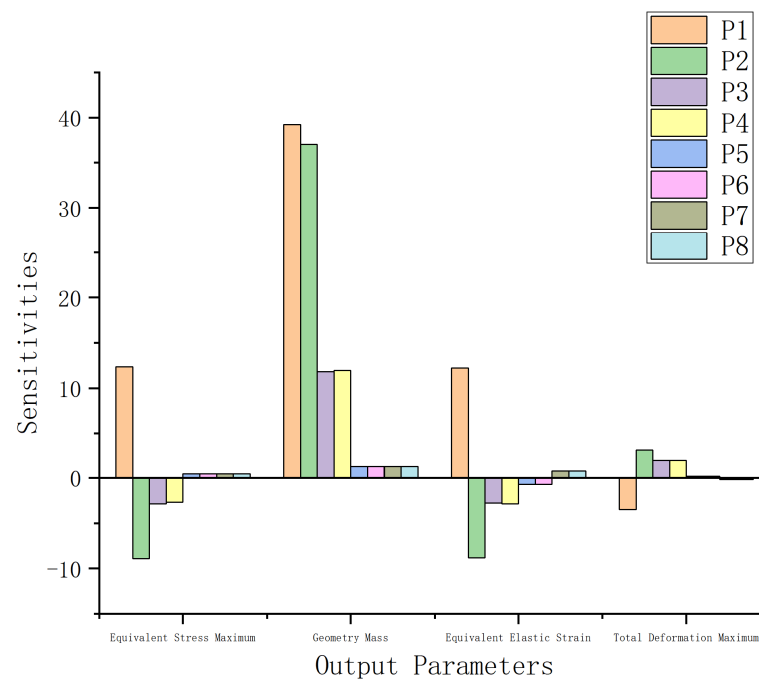


**Figure 8.** Frame's local sensitivity.

Overall, the upper and lower limits of the design variables P1–P4 were set to  $\pm 15\%$  of the original parameters because of the more significant influence that the frame bracket arms and external reinforcement plates have on the frame. Subsequently, according to the manufacturer's requirements and the actual situation, the specific variation ranges of these four design variables were determined, as detailed in Table 4.

**Table 4.** Vehicle frame initial design variables.

Initializing Variable	Size	Variation Range
P1	25	20~27
P2	25	20~27
P3	25	23~27
P4	25	23~27

### 5.2. Latin Hypercube Experimental Design

It is necessary to choose reasonable experimental design methods before establishing the Kriging model. Typical methods include the Latin Hypercubic Design of Experiments (LHD), the Full Factorial Design of Experiments (FFD), the Orthogonal Design of Experiments (OD), the Uniform Design of Experiments (UD), etc. [28]. These points should reflect the characteristics of the design space as much as possible, as this is related to the accuracy of the approximate model. Unlike random sampling, Latin Hypercubic Sampling (LHS), a kind of stratified random sampling, can guarantee the full coverage of each variable's range by optimizing the stratification of each marginal distribution. It can sample from the distributional intervals of the variables with efficiency. Consequently, as illustrated in Figure 9, 25 sample points are chosen using Latin Hypercubic Sampling in this work to obtain two-dimensional sampling results.

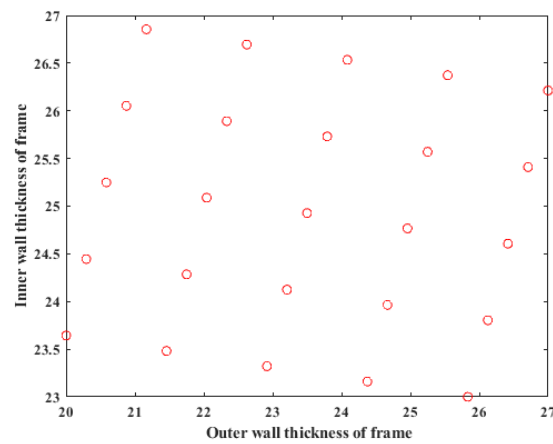


**Figure 9.** The results of the Latin Hypercube Sampling experimental design. (The red circles in the figure indicate design variables.).

### 5.3. The Construction of the Kriging Model

The above sample values are given to the frame's finite element model for calculation, and the output values are obtained. The 25 sample points obtained above are used as the initial training samples, and another 10 sample points are extracted to test the Kriging model. The Kriging model is constructed using Matlab2018a's Dace toolbox. The sample and output values mentioned above are brought into the program for calculation, and the resulting prediction plots of the maximum stress and frame weight are displayed in Figures 10 and 11, respectively.

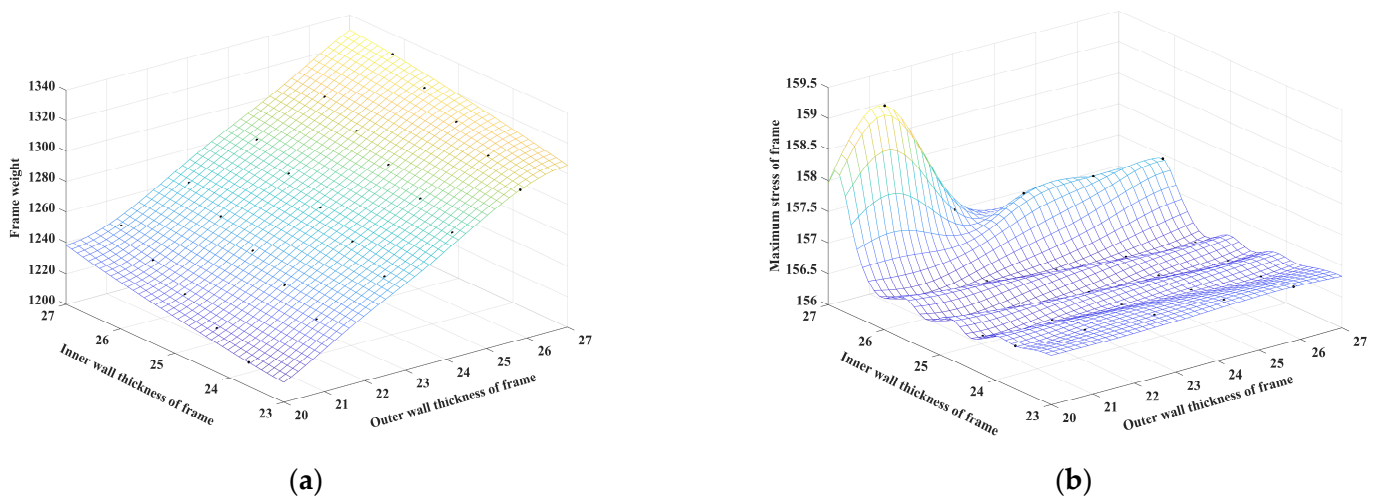


**Figure 10.** Kriging approximate prediction model. (a) Kriging approximation model prediction of frame weights. (b) Kriging approximation model prediction of maximum stress value.

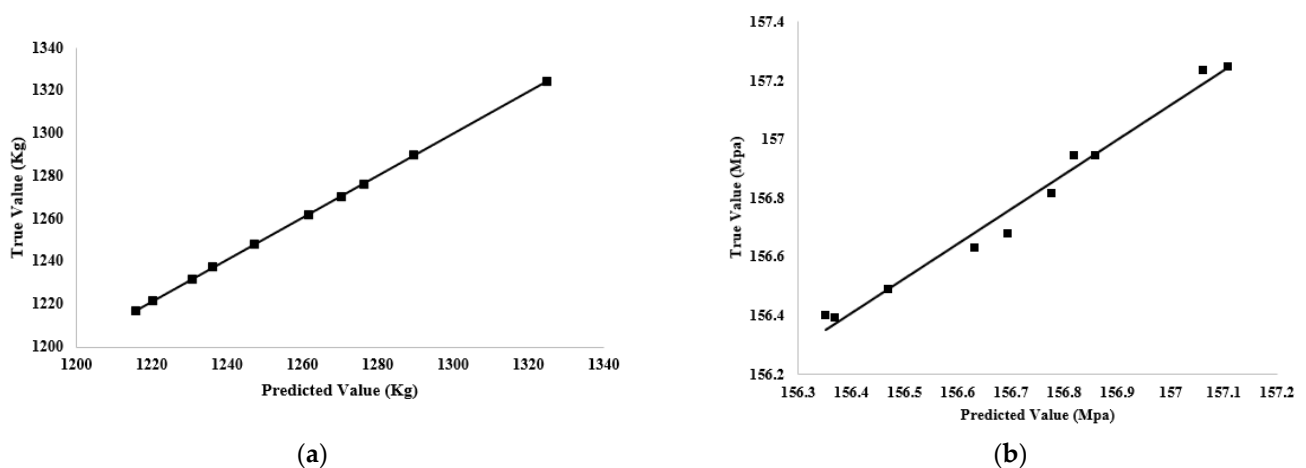


**Figure 11.** Surrogate model accuracy check. (a) Frame weight. (b) Maximum frame stress.

#### 5.4. Accuracy Evaluation of Kriging Model

An additional 10 sample points from the Kriging model prediction result values and the actual result values were taken to test the surrogate model's accuracy. The approximation model can be tested by the coefficient of determination,  $R^2$ , the expression of which is shown in Equation (19).

$$R^2 = 1 - \frac{\sum_i (y_i - \hat{y}_i)^2}{\sum_i (y_i - \bar{y}_i)^2} \quad (19)$$

where  $y_i$  is the calculated value of the sample point;  $\hat{y}_i$  is the predicted value of the model; and  $\bar{y}_i$  is the mean value.

The coefficient of determination,  $R^2$ , has a size ranging from 0 to 1. The model is more accurate at representing the real value when the  $R^2$  value is closer to 1. Through the examination of the 10 sample points, the Kriging models of the frame weight ( $R^2 = 0.9999$ ) and the frame maximum stress ( $R^2 = 0.9809$ ) are obtained. The coefficient of determination of this surrogate model is close to 1, indicating that the frame model has a high fitting accuracy, and both meet the accuracy requirements for constructing the surrogate model in the project. Figure 11 displays the error analysis of the Kriging model for both the frame mass and the maximum stress of the frame.

## 6. Multi-Objective Optimization

Following a thorough analysis of the frame's overall mass parameter and maximum stress parameter, multi-objective optimization is performed for the bracket arms and reinforcing plates on both sides of the frame. The optimization model can be characterized as follows, with the minimum mass of the frame and the maximum stress of the frame not exceeding the yield strength of the material serving as the optimization objectives.

$$\left\{ \begin{array}{l} \text{find : } P = (P_1, P_2, P_3, \dots, P_i) \\ \text{Min : } \{m(x), \sigma(x)\} \\ \text{s.t. } \sigma \leq 235 \text{ Mpa} \\ P_L \leq P \leq P_U \end{array} \right. \quad (20)$$

where  $P$ —the frame design variable;

$m(x)$ —the overall weight of the frame;

$\sigma(x)$ —the maximum stress of the frame;

$P_L, P_U$ —the upper and lower limit values of the design variables.

A general multi-objective optimization problem's solution set is typically the Pareto optimal solution set or the set of non-inferior solutions. MOGA is a fast non-dominated

sorting technique that is a hybrid version of the NSGA-II algorithm based on the Control Elite strategy. It supports a wide range of input parameter types.

The initial sample count is set to 2000, and the maximum number of iterations is set to 200. The Pareto front can be obtained by solving using MOGA, as shown in Figure 12, and the five candidate analyses obtained by the optimization calculation are shown in Table 5.

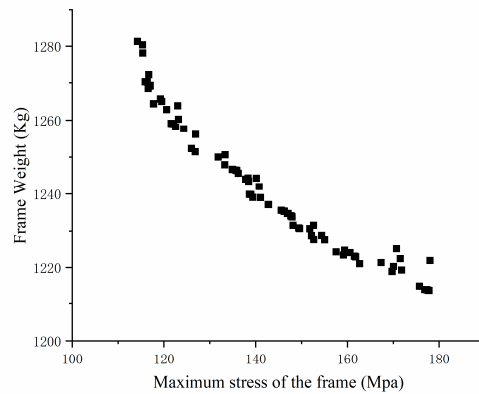


Figure 12. Pareto frontier.

Table 5. Multi-objective optimization results.

Variables	Scheme 1	Scheme 2	Scheme 3	Scheme 4	Scheme 5
P1/mm	20.021	20.501	21.035	22.028	22.528
P2/mm	20.021	20.501	21.035	22.028	22.528
P3/mm	23.345	23.109	24.107	24.513	25.013
P4/mm	23.345	23.109	24.107	24.513	25.013
Frame weight/Kg	1214.4	1219	1232	1248	1257
Maximum stress of frame/MPa	177.07	176.48	175.87	173.53	169.19

### 7. Optimal Solution of Frame Structure Parameters

#### 7.1. Hierarchical Structure Model Establishment

As illustrated in Figure 13, the objective layer, criterion layer, and scheme layer comprise the hierarchical model to optimize the structural parameters of the automatic loading and unloading mixer truck’s frame. The four optimization objectives—the frame mass, maximum stress, maximum strain, and first-order inherent frequency of the frame—make up the criterion layer; the five groups of optimization schemes produced by the multi-objective genetic algorithm comprise the scheme layer. The total objective layer is the optimal design scheme of the frame’s structural parameters.

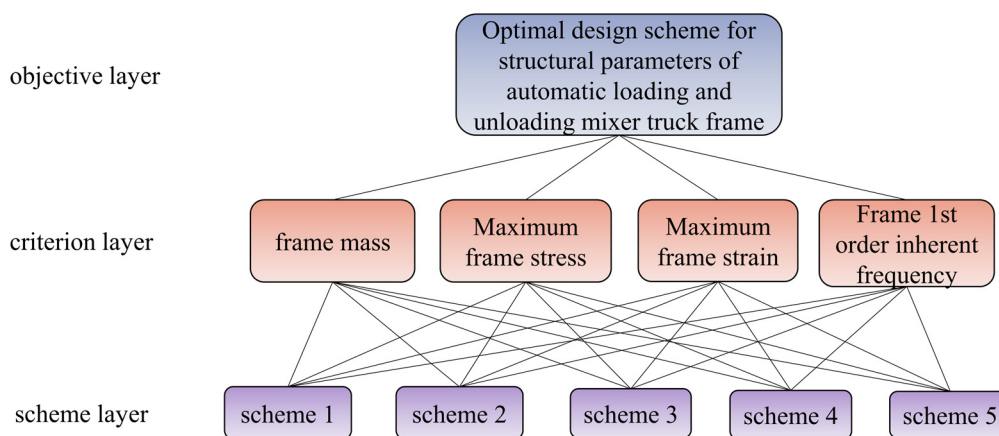


Figure 13. Hierarchical model for optimization of frame structure parameters.

### 7.2. Priority Matrix Construction of Scheme Layer

The scheme layer is constructed under the premise of meeting the strength and dynamic characteristics of the frame of the automatic loading and unloading mixer truck. In other words, the larger the inverse of the frame mass, the better. Equation (21) displays the mass inverse matrix  $N_m$  of the six groups of optimization schemes that are obtained through optimization.

$$N_m = \begin{pmatrix} 0.0008235, & 0.0008203, & 0.0008117, \\ & & & & & \\ & & & 0.0008013, & & & \\ & & & & 0.0007955 & & \end{pmatrix} \quad (21)$$

By comparing the elements of the mass inverse matrix  $N_m$  shown in Equation (21) two by two, the matrix  $W_m$  is obtained, as shown in Equation (22).

$$W_m = \begin{bmatrix} 1 & 1.0039 & 1.0145 & 1.0277 & 1.0352 \\ 0.9961 & 1 & 1.0106 & 1.0237 & 1.0312 \\ 0.9857 & 0.9895 & 1 & 1.0130 & 1.0204 \\ 0.9730 & 0.9768 & 0.9872 & 1 & 1.0073 \\ 0.9660 & 0.9698 & 0.9800 & 0.9928 & 1 \end{bmatrix} \quad (22)$$

Summing the data of the columns of the matrix  $W_m$  shown in Equation (22) yields the matrix  $Q_m$ , as shown in Equation (23).

$$Q_m = (4.9208, 4.9400, 4.9923, 5.0572, 5.0941) \quad (23)$$

The data in each column of matrix  $W_m$  are divided by the data in the corresponding column of matrix  $Q_m$ , and the quotient obtained is summed and averaged to obtain the prioritization matrix  $P_m$  of the frame quality, as shown in Equation (24).

$$P_m = (0.9972, 1.0010, 1.0121, 1.0406, 1.0572) \quad (24)$$

Similarly, the priority matrices  $P_\sigma$ ,  $P_\varepsilon$ , and  $P_{f1}$  of the maximum stress and maximum strain of the frame with respect to the first-order intrinsic frequency can be obtained as shown in Equation (25) to Equation (27).

$$P_\sigma = (0.9979, 0.9973, 0.9970, 1.0001, 1.0134) \quad (25)$$

$$P_\varepsilon = (1.0208, 0.9997, 0.9988, 0.9919, 0.9768) \quad (26)$$

$$P_{f1} = (0.2130, 0.2092, 0.2026, 0.1961, 0.1952) \quad (27)$$

The final prioritization matrix  $P$  for the scenario layer is obtained as shown in Equation (28).

$$P = [P_m, P_\sigma, P_\varepsilon, P_{f1}]^T \quad (28)$$

### 7.3. Judgment Matrix Construction of Criterion Layer

The "1–9 scale method" is utilized to establish the judgment matrix of the criterion layer. Reducing the mass of the frame is the main goal when optimizing its structural parameters; for this reason, the mass of the frame, its maximum stress, maximum strain, and first-order intrinsic frequency are taken as 5, 3, and 3, respectively. The dynamic characteristics of the entire machine are directly affected by the maximum strain of the frame and the first-order intrinsic frequency of the frame. For this reason, the maximum strain of the frame, the frame of the first-order intrinsic frequency of the frame, and the frame of the maximum stress of the corresponding scale are taken as 1/3 and 1/3, respectively. The maximum strain of the frame and the frame of the first-order intrinsic

frequency are taken as 1, which can be used to obtain the judgment matrix  $I$ , as shown in Equation (29).

$$I = \begin{bmatrix} 1 & 5 & 3 & 3 \\ 0.2 & 1 & 0.333 & 0.333 \\ 0.333 & 3 & 1 & 1 \\ 0.333 & 3 & 1 & 1 \end{bmatrix} \quad (29)$$

The maximum characteristic root  $\lambda_{max} = 4.043$  of the judgment matrix  $I$  and its corresponding regularized eigenvector  $W$ , i.e., the weight matrix  $W$ , can be derived.

$$W = (0.5194, 0.7887, 0.2009, 0.2009) \quad (30)$$

#### 7.4. Consistency Test for Judgment Matrices

According to Equation (31), the consistency index  $CI$  of the judgment matrix  $I$  can be calculated as 0.014. The closer the value of the consistency index  $CI$  is to 0, the better the consistency of the judgment matrix  $I$  is.

$$CI = \frac{\lambda_{max} - n}{n - 1} \quad (31)$$

where  $n$ —the judgment matrix dimension;

$\lambda_{max}$ —the judgment matrix  $I$  maximum characteristic root.

To be able to accurately evaluate the consistency of the judgment matrix, the mean random consistency index  $RI$  is introduced, and according to  $n = 4$ , it can be seen that  $RI = 0.882$ . According to Equation (32), the judgment according to the consistency ratio,  $CR$ , is calculated and judged.

$$CR = \frac{CI}{RI} \quad (32)$$

The above yields  $CR = 0.016$ ; since  $CR < 0.1$ , the consistency of the judgment matrix  $I$  is satisfied.

#### 7.5. Optimal Solution Determination

Multiplying the priority matrix  $P$  at the scheme level with the judgment matrix  $W$  at the criterion level yields the judging criteria priority matrix  $A$  for the five optimization schemes.

$$A = W \times P = (1.58383306, 1.5533799, 1.56793571, 1.55285983, 1.54935792) \quad (33)$$

According to the calculation results of Equation (33), it can be concluded that the priorities of the five design schemes for optimizing the structural parameters of the mixer truck frame are, in order, Scheme 1, Scheme 3, Scheme 2, Scheme 4, and Scheme 5. Therefore, Scheme 1 is selected as the optimal design scheme, and the weights, maximum stresses, safety factors, maximum strains, and first-order intrinsic frequencies of the frames before and after optimization are shown in Table 6.

**Table 6.** Comparison of results before and after frame size optimization.

Variables	Pre-Optimization	Post-Optimization	Rate of Change/%
Frame weight/kg	1292.8	1214.4	−6.06
Maximum stress/MPa	158.28	177.07	+11.87
Safety factor	1.48	1.33	−10.14
Maximum strain	0.00068332	0.00086195	+26.14
First natural frequency/Hz	8.9373	9.1682	+2.58

As can be seen from Table 6, the weight of the frame after size optimization is reduced from 1292.8 kg to 1214.4 kg, which is a 6.06% reduction; the maximum stress of the frame is increased from 158.28 Mpa to 177.07 Mpa, which is an 11.87% reduction, but it is still

in the permissible stress of the frame within 235 Mpa; the minimum safety factor of the frame is reduced from 1.48 to 1.33, which is a 10.14% reduction; the maximum strain of the frame is increased from 0.00068332 to 0.00086195, which is a 26.14% increase; and the first-order intrinsic frequency of the frame is increased from 8.94 Hz to 9.08 Hz, which is a 1.57% increase. Since the maximum strain was 0.00086195, which increased by 26.14%, the frame's first-order intrinsic frequency increased from 8.9373 Hz to 9.1682 Hz, which is a 2.58% increase. It is clear that the frame's structural parameters have been optimized to ensure that the maximum stress it can withstand falls within the structure's allowable stress range, reduces the mass, and enhances the frame's structural modal characteristics by raising the low-order intrinsic frequency.

### 7.6. Comparison of Optimization Methods

Therefore, the performance evaluation of the Kriging + AHP model was further deepened by considering the whole optimization process. Compared with the single Kriging surrogate model and the AHP model, the hybrid Kriging + AHP model exhibits higher efficiency and accuracy in optimization, as shown in Figure 14. The figure illustrates the iterative curves of the three models for frame weight, where the green curve represents the Kriging + AHP model, the orange curve represents the AHP model alone, and the red curve represents the Kriging model alone. It is observed that the AHP model is relatively slower in the first five iterations, but its optimization results are better; on the contrary, the Kriging model is faster in the first five iterations, but its final optimization results are relatively worse.

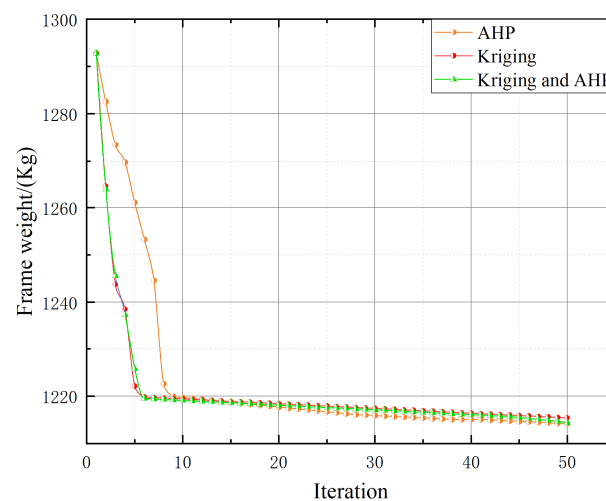


**Figure 14.** Comparison of three model iteration curves.

The hybrid Kriging + AHP model incorporates the advantages of both, which not only shows faster speed in the first five steps of iteration, but also shows that the final optimization results are reasonable. By calculation, it can be concluded that the first five steps of the iteration hybrid model has approximately doubled the optimization efficiency compared to the AHP model, and the accuracy of the final optimization result is improved by 3.6% for the hybrid model compared to the Kriging model. Therefore, this proves that the hybrid Kriging + AHP model cleverly combines the advantages of both, guiding the optimization process in a more efficient and accurate manner, ensuring more desirable results throughout the iterations. This further solidifies the excellence of the Kriging + AHP model in optimization.

## 8. Topology Optimization of Mixer Truck Frame

Through the above optimization of the frame size, the reduction in the thickness of the frame bracket arm is realized. However, the frame structure obtained by size optimization

only reduces the thickness of some parts in the frame and cannot be used as the result of the final design. Therefore, it is also necessary to carry out topology optimization on the structure based on the frame size optimization.

Topology optimization can further optimize the structure of the frame and find the optimal material distribution scheme in the optimization space of uniform materials. The scheme is reflected as a “maximum stiffness” design in topology optimization. On the basis of size optimization, it is made more lightweight with higher strength and better stiffness while reducing material waste and manufacturing costs. In addition, topology optimization can also reduce noise and vibration and improve the comfort and stability of the frame, thereby improving the performance and safety of the vehicle. After considering the structural performance requirements, weight optimization manufacturing feasibility, cost, etc., this paper uses three schemes for topology optimization; compares the material density change thresholds of 0.2, 0.4, and 0.5; and then selects the best among them. The division results of the frame optimization design domain are shown in Figure 15, where the tank arm on both sides of the frame is the design domain, and the rest of the area is the non-design domain.

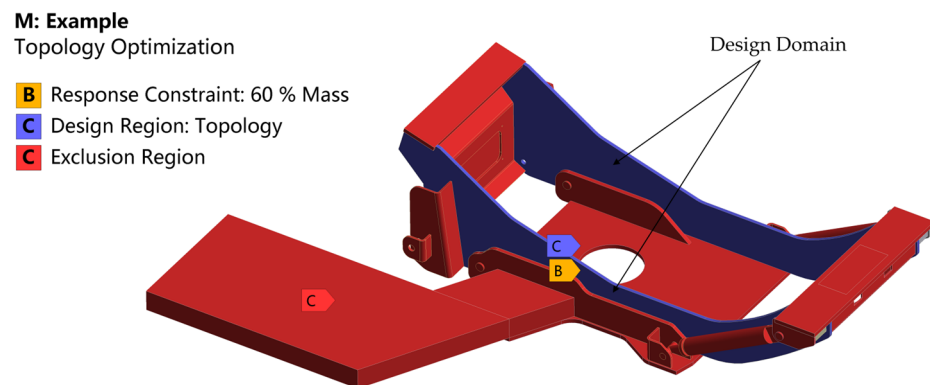


**Figure 15.** Frame topology optimization design domain.

The topology optimization results for setting the material density change thresholds to 0.2, 0.4, and 0.5 are shown in Figures 16–18. Considering the feasibility and performance of the frame, the topology optimization with a threshold of 0.4 results in a balance between feasibility and performance. Lower thresholds may lead to excessive material removal, resulting in structural fragility or instability, while higher thresholds may retain too much material, limiting performance gains. Selecting a threshold of 0.4 can achieve a higher level of optimization performance while maintaining structural feasibility.

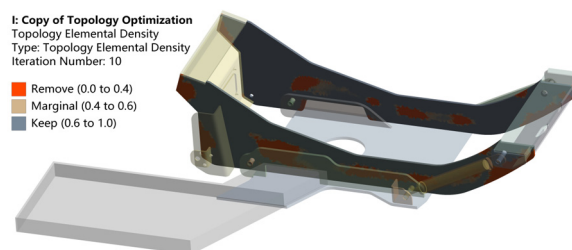


**Figure 16.** Threshold of 0.2.

According to the topology optimization results with a threshold of 0.4, and considering the processing property of the frame, the optimized area is reasonably removed, and the frame structure of the automatic loading and unloading mixer truck after topology optimization is obtained, as shown in Figure 19. The comparison reveals that the topology-optimized frame structure has achieved weight reduction by digging some polygonal holes in the non-assembled areas. After the optimization, the bracket arm on both sides of the

frame is reduced by 76.207 Kg compared with that before optimization, and the overall weight of the frame is reduced by 11.96% compared with that before optimization.

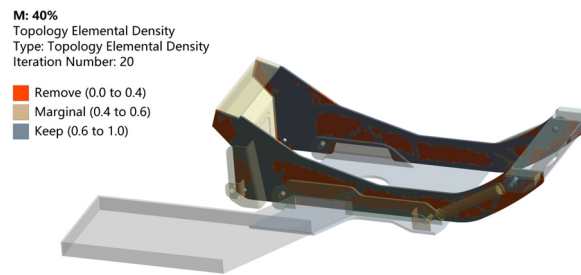


Figure 17. Threshold of 0.4.

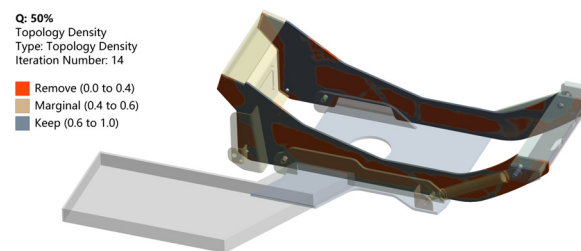


Figure 18. Threshold of 0.5.

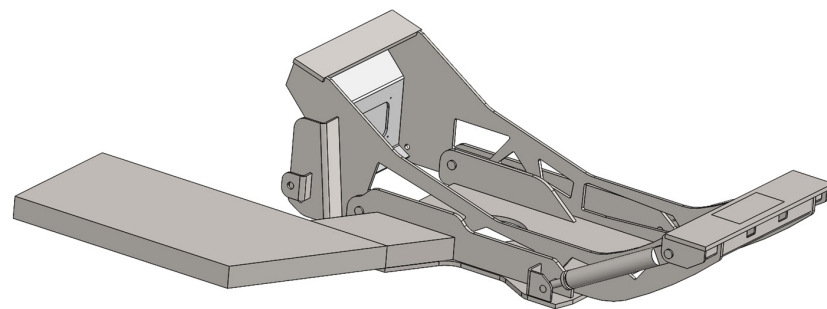


Figure 19. Structure after topology optimization.

After the optimization of the frame of the first 15 orders of modes, shown in Table 7, it can be seen that 1~6 orders are also rigid body modes, the frequency of the first 10 orders is lower than the frequency of the engine idling, and the frequency of the last 5 orders is also lower than the frequency of the engine that commonly used. Additionally, it can be seen in Table 7 that the frequency of the frame of the various orders of changes in the stability of the phenomenon does not have prominence. Based on the above analysis, the design of the frame is reasonable and meets the requirements of the vehicle.

Table 7. Fifteenth-order modal analysis of optimized frame.

Ordinal Number	Frequency/Hz
1~6	0
7	9.17
8	16.9
9	19.8
10	23.7
11	25.3
12	28.0
13	30.9
14	40.4
15	44.4

After size optimization and topology optimization, the overall optimized frame performance was significantly changed, as shown in Table 8, where the weight, maximum stress, factor of safety, maximum strain, and first-order intrinsic frequency of the frame were again changed.

**Table 8.** Comparison of results before and after frame topology optimization.

Variables	Pre-Optimization	Post-Optimization	Rate of Change/%
Frame weight/kg	1214.4	1138.2	−6.27
Maximum stress/MPa	177.07	183.39	+3.57
Safety factor	1.33	1.28	−3.76
Maximum strain	0.00086195	0.00092352	+7.14
First natural frequency/Hz	9.08	9.17	+0.99

By comparing the data in Table 8, it can be seen that the topology optimization had a significant impact on the performance of the frame. After size optimization, the total weight of the frame was reduced from 1214.4 kg to 1138.2 kg, which is a 6.27% reduction. In addition, the maximum stress of the frame increased from 177.07 Mpa to 183.39 Mpa, which is a 3.57% increase, but it still stays within the permissible stress of the frame, which is not more than 235 Mpa. The minimum safety factor of the frame also decreased slightly, from 1.33 to 1.28, which is a 3.76% decrease. Meanwhile, the maximum strain of the frame is increased from 0.00086195 to 0.00092352 after topology optimization, which is a significant increase of 7.14%. In terms of the structural dynamic characteristics, the first-order intrinsic frequency of the frame is slightly increased from 9.08 Hz before optimization to 9.17 Hz, which is an increase of 0.99%.

The results of this series of optimizations show that the structure of the frame is effectively improved through topology optimization. The maximum stress is still within the allowable stress range of the structure, the mass is reduced, and the dynamic response of the structure is also improved. This not only provides a feasible way to improve the performance of the vehicle, but also provides a useful reference for the optimization of the structure of similar electric vehicles in the design stage.

The optimized frame was assembled to the mixer truck and tested again for working condition b, or bucket lift. Figure 20a presents the results of the size-optimized test, representing the scenario where the mixer truck is on a 15-degree slope with the bucket in a flat position. The optimized chassis demonstrated excellent performance under this condition, showing no signs of bending or fracture.



**Figure 20.** Experimental verification of working condition b. (a) Mixer truck uphill 15 degrees and bucket flat. (b) Mixer truck with upper load rotated 90 degrees and bucket flat. (c) Mixer truck at rest with the bucket flat.

Additionally, the independent test depicted in Figure 20b involves rotating the upper part of the mixer truck by 90 degrees with the bucket in a flat position, and similarly, no failure was observed. Meanwhile, Figure 20c illustrates the comprehensive test of the mixer

truck chassis after size and topology optimizations, simulating the scenario where the bucket is full and in a flat position during operation. In this comprehensive test, neither structural nor material failure occurred, laying a solid foundation for the reliability of future lightweight electric chassis. These test results strongly validate the credibility of our optimization strategy, providing robust support for future chassis design.

## 9. Conclusions

Taking the frame of the automatic loading and unloading mixer truck as the research example, this paper proposes the design optimization of the structural parameters of the frame based on the combination of the Kriging model and hierarchical analysis method, and on this basis, the material distribution of the frame is optimized by using topology optimization, which provides an efficient optimization design method to make the frame of the electric vehicle lightweight. The following conclusions can be drawn:

(1) On the basis of the in-depth analysis of the overall load-bearing performance of the automatic loading and unloading mixer truck, the frame was subjected to a multi-case stress analysis and static finite element analysis so as to identify the most dangerous working conditions. Secondly, the structural modal characteristics of the frame were studied before optimization, which paved the way for the subsequent refined size optimization and optimization strategy with topological features.

(2) In order to improve the efficiency and accuracy of the optimization of the frame's structural parameters, the structural parameters that have significant influences on the frame's weight, structural static characteristics, and structural modal characteristics are screened out as design variables through a sensitivity analysis. An approximate model of the frame's weight and maximum stress is constructed by using the Kriging model, and a hybrid model based on the combination of the Kriging model and hierarchical analysis is used to optimize the frame with the objectives of a minimum frame mass and maximum stress. By comparing the iterative curves of the hybrid model and the single model in terms of the frame's weight, it can be concluded that the initial optimization efficiency of the hybrid model is about double compared with that of the AHP model, and the final optimization result of the hybrid model is about 3.6% higher compared with that of the Kriging model, which proves that this method can be used as an effective tool for the multi-objective optimization of electric vehicle frames and can provide higher efficiency and accuracy.

(3) The structural parameters of the frame are comprehensively improved by integrating the two methods of size optimization and topology optimization. This integrated optimization method significantly improves the optimization efficiency and accuracy. The results show that during the size optimization stage, the thickness of the key components of the frame is reduced by 78.4 Kg, and although the maximum stress of the frame rises from 152.28 MPa to 177.07 MPa, it is still within the allowable stress range (235 MPa). The correctness of the size optimization was verified in subsequent frame experiments. Subsequently, through topology optimization, the weight of the bracket arms on both sides of the frame was reduced by 76.2 Kg. The maximum stress of the frame increased from 177.07 MPa to 183.39 MPa, which, again, did not exceed the allowable stress of the material. Through the field experiments of the frame under working condition b, it was found that the frame shows good performance under load conditions, which further verifies its reliability under actual working conditions. In summary, this method not only provides a new idea for the optimization design of electric vehicle components, but also has a wide application potential and provides a useful reference for engineering practice and technical research in the field of electric vehicles.

**Author Contributions:** Conceptualization, X.Y. and Q.H.; methodology, Q.H., X.Y. and H.W.; software, Q.H.; validation, X.L., W.M. and H.W.; formal analysis, X.L.; investigation, W.M.; resources, Q.H. and X.L.; data curation, X.L. and W.M.; writing—original draft preparation, Q.H.; writing—review and editing, X.L.; visualization, W.M.; supervision, H.W.; project administration, X.Y.; funding acquisition, X.Y. All authors have read and agreed to the published version of the manuscript.

**Funding:** This research was funded by the National Natural Science Foundation of China, grant number 52005305.

**Data Availability Statement:** The original contributions presented in the study are included in the article, further inquiries can be directed to the corresponding author.

**Conflicts of Interest:** The authors declare no conflicts of interest.

## Abbreviations

The following abbreviations are used in this manuscript:

AHP	Analytic Hierarchy Process
FEA	Finite Element Analysis
ESO	Evolutionary Structural Optimization
ICM	Independent Continuous Mapping
SIMP	Solid Isotropic Materials with Penalties
CHP	Combined Heat and Power
PEVs	Plug-in Electric Vehicles
OSTFOF	Optimal Self-Tuning Fractional Order Fuzzy
PFA	Path-finding Algorithm
PI	Proportional Integral
PID	Proportion Integration Differentiation
FOPID	Fractional Order PID
DG	Distributed Generation
EVs	Electric Vehicles
MMA	Method of Moving Asymptotes
LP	Linear Programming
HETOP	Hybrid Element Topology Optimization
ANN	Artificial Neural Network
RBF	Radial Basis Functions
SVM	Support Vector Machine
PRG	Polynomial Regression
LHD	Latin Hypercubic Design
FFD	Full Factorial Design
OD	Orthogonal Design
UD	Uniform Design
LHS	Latin Hypercubic Sampling
MOGA	Multi-Objective Genetic Algorithm
NSGA-II	Non-Dominated Sorting Genetic Algorithm II
CI	Consistency Index
RI	Random Consistency Index
CR	Consistency Ratio
Variable	Description
$z(x)$	Gaussian stochastic function
$y(x)$	function estimate of the unknown point
$f(x)$	linear regression function
$\beta$	regression coefficient
$\hat{f}(x)$	estimate of $f(x)$
$w = (w_1, w_2, \dots, w_n)^T$	vector of weighting coefficients to be solved
$y = (y^1, y^2, \dots, y^n)^T$	known sample point data
$R = [R_{ij}] = [R(c, x^i, x^j)], (i, j = 1, 2, \dots, n)$	correlation function using the kernel function as Gaussian function
$r = (R(c, x, x^1), \dots, (R(c, x, x^n))^T, R(c, x, x^i)$	correlation function using the kernel function as Gaussian function
$d_j$	distance between the point to be measured and the sample point

$c_j$	constant covariate of the kernel function in the $j$ th direction of the sample point
$w$	weighting coefficients
$x$	vector of design variables
$c_i(x)$	inequality constraint
$h_j(x)$	equation constraint functions
$x_{min}$	lower limit of design variable
$x_{max}$	upper limit of design variables
$\rho$	design variable
$\rho_{min}$	minimum density
$\rho_i$	relative density
$V_i$	relative volume
$m$	objective function
$S$	stresses
$G$	deformations
$C$	topology-optimized design domain of the frame
$M$	mass of the mixing cylinder when it is fully loaded
$A_x$	gravitational acceleration parallel to the X-axis
$A_y$	gravitational acceleration parallel to the Y-axis
$A_z$	parallel Z-axis of the gravitational acceleration
$l$	distance
$\theta$	angle
$M_C$	torque
$F$	force
$y_i$	calculated value of the sample point
$\hat{y}_i$	predicted value of the model
$\bar{y}_i$	mean value
$P$	frame design variable
$m(x)$	overall weight of the frame
$\sigma(x)$	maximum stress of the frame
$P_L, P_U$	upper and lower limit values of design variables
$N_m$	mass inverse matrix
$n$	judgment matrix dimension
$\lambda_{max}$	judgment matrix $I$ maximum characteristic root

## References

- Zou, Y.; Sun, F.; Hu, X.; Guzzella, L.; Peng, H. Combined Optimal Sizing and Control for a Hybrid Tracked Vehicle. *Energies* **2012**, *5*, 4697–4710. [[CrossRef](#)]
- Tyflopoulos, E.; Steinert, M. Topology and Parametric Optimization-Based Design Processes for Lightweight Structures. *Appl. Sci.* **2020**, *10*, 4496. [[CrossRef](#)]
- Wu, J.; Sigmund, O.; Groen, J.P. Topology optimization of multi-scale structures: A review. *Struct. Multidiscip. Optim.* **2021**, *63*, 1455–1480. [[CrossRef](#)]
- Bendsøe, M.P.; Kikuchi, N. Generating Optimal Topologies in Structural Design Using A Homogenization Method. *Comput. Methods Appl. Mech. Eng.* **1988**, *71*, 197–224. [[CrossRef](#)]
- Bendsoe, M.P. Optimal shape design as a material distribution problem. *Struct. Optim.* **1989**, *1*, 193–202. [[CrossRef](#)]
- Xie, Y.M.; Steven, G.P. A Simple Evolutionary Procedure for Structural Optimization. *Comput. Struct.* **1993**, *5*, 885–896. [[CrossRef](#)]
- Bendsøe, M.P.; Sigmund, O. Material interpolation schemes in topology optimization. *Arch. Appl. Mech.* **1999**, *69*, 635–654. [[CrossRef](#)]
- Dilgen, S.B.; Dilgen, C.B.; Fuhrman, D.R.; Sigmund, O.; Lazarov, B.S. Density based topology optimization of turbulent flow heat transfer systems. *Struct. Multidiscip. Optim.* **2018**, *57*, 1905–1918. [[CrossRef](#)]
- Zhang, S.; Norato, J.A. Finding Better Local Optima in Topology Optimization via Tunneling. In Proceedings of the International Design Engineering Technical Conferences and Computers and Information in Engineering Conference, Quebec City, QC, Canada, 26–29 August 2018; Volume 8, p. V02BT03A014.
- Sosnovik, I.; Oseledets, I. Neural networks for topology optimization. *J. Numer. Anal. Math. Model.* **2019**, *34*, 215–223. [[CrossRef](#)]

11. Gomes, P.; Palacios, R. Aerodynamic-driven topology optimization of compliant airfoils. *Struct. Multidiscip. Optim.* **2020**, *62*, 2117–2130. [[CrossRef](#)]
12. Al-Shahri, O.A.; Ismail, F.B.; Hannan, M.; Lipu, M.H.; Al-Shetwi, A.Q.; Begum, R.; Al-Muhsen, N.F.; Soujeri, E. Solar photovoltaic energy optimization methods, challenges and issues: A comprehensive review. *J. Clean. Prod.* **2021**, *284*, 125465. [[CrossRef](#)]
13. Liu, W.K.; Li, S.; Park, H.S. Eighty years of the finite element method: Birth, evolution, and future. *Arch. Comput. Methods Eng.* **2022**, *29*, 4431–4453. [[CrossRef](#)]
14. Rozvany, G.I.N.; Birker, T. On singular topologies in exact layout optimization. *Struct. Optim.* **1994**, *8*, 228–235. [[CrossRef](#)]
15. Marler, R.T.; Arora, J.S. Survey of multi-objective optimization methods for engineering. *Struct. Multidiscip. Optim.* **2004**, *26*, 369–395. [[CrossRef](#)]
16. Sobieski, J.S. Two alternative ways for solving the coordination problem in multilevel optimization. *Struct. Optim.* **1993**, *6*, 205–215. [[CrossRef](#)]
17. Zamani, A.A.; Shafiee, M.; Sajadinia, M. Optimal self-tuning fractional order fuzzy Load Frequency Control considering sustainable energy sources and electric vehicle. *Int. J. Ambient Energy* **2023**, *44*, 2170–2184. [[CrossRef](#)]
18. Mohanty, D.; Panda, S. Modified salp swarm algorithm-optimized fractional-order adaptive fuzzy PID controller for frequency regulation of hybrid power system with electric vehicle. *J. Control Autom. Electr. Syst.* **2021**, *32*, 416–438. [[CrossRef](#)]
19. Shafiee, M.; Ghazi, R.; Moeini-Aghaie, M. A multi-objective framework for energy resource scheduling in active distribution networks. *Int. J. Ambient Energy* **2019**, *40*, 504–516. [[CrossRef](#)]
20. Han, Z. Kriging surrogate model and its application to design optimization: A review of recent progress. *Acta Aeronaut. Astronaut. Sin.* **2016**, *37*, 3197–3225.
21. Mu, X.; Yao, W.; Yu, X.; Liu, K.; Xue, F. A survey of surrogate models used in MDO. *Chin. J. Comput. Mech.* **2005**, *22*, 608–612.
22. Duan, B.; Ye, S. Comparison of Topology Optimization Design Methods for Bar Structures. *Electro-Mech. Eng.* **1989**, *29*, 1525–1567.
23. Xue, H.; Yu, H.; Zhang, X.; Quan, Q. A Novel Method for Structural Lightweight Design with Topology Optimization. *Energies* **2021**, *14*, 4367. [[CrossRef](#)]
24. Jiao, H.; Zhou, Q.; Li, Q.; Li, Y. Periodic Topology Optimization Using Variable Density Method. *J. Mech. Eng.* **2013**, *49*, 132–138. [[CrossRef](#)]
25. Zhou, K. A Review on Topology Optimization of Structures. *Adv. Mech.* **2005**, *35*, 69–76.
26. GB/T 26408-2011; Concrete Tuck Mixer. China Standard Publishing House: Beijing, China, 2011.
27. Guan, C.; Zhang, H.; Wang, X.; Miao, H.; Zhou, L.; Liu, F. Experimental and Theoretical Modal Analysis of Full-Sized Wood Composite Panels Supported on Four Nodes. *Materials* **2017**, *10*, 683. [[CrossRef](#)]
28. Zhang, J.; Xu, J.; Jia, K.; Yin, Y.; Wang, Z. Optimal Sliced Latin Hypercube Designs with Slices of Arbitrary Run Sizes. *Mathematics* **2019**, *7*, 854. [[CrossRef](#)]

**Disclaimer/Publisher’s Note:** The statements, opinions and data contained in all publications are solely those of the individual author(s) and contributor(s) and not of MDPI and/or the editor(s). MDPI and/or the editor(s) disclaim responsibility for any injury to people or property resulting from any ideas, methods, instructions or products referred to in the content.